Journal of The Electrochemical Society, **163** (8) F867-F871 (2016)
0013-4651/2016/163(8)/F867/5/$33.00 © The Electrochemical Society

Electrochemical Characterization of Carbon Nanotube and Poly (3,4-ethylenedioxythiophene)−Poly(styrenesulfonate) Composite Aqueous Electrolyte for Thermo-Electrochemical Cells

Ali H. Kazim[a,*] **and Baratunde A. Cola**[a,b,**,z]

[a]*George W. Woodruff School of Mechanical Engineering, Georgia Institute of Technology, Atlanta, Georgia 30332, USA*
[b]*School of Materials Science and Engineering, Georgia Institute of Technology, Atlanta, Georgia 30332, USA*

Aqueous potassium ferri/ferrocyanide electrolyte has been the standard electrolyte for thermo-electrochemical cells due to its high seebeck coefficient and high current exchange density. Here, the effect of mixing carbon nanotubes and poly (3,4-ethylenedioxythiophene)−poly(styrenesulfonate) in aqueous potassium ferri/ferrocyanide electrolyte is characterized using electrochemical impedance spectroscopy. Analysis of the impedance spectra shows a 10% increase in ohmic conductivity and about 5-fold decrease in interfacial charge transfer resistance in the composite electrolyte, which is caused by addition of charge carriers, interfacial polarization and improved contact at the electrode/electrolyte interface. The enhancement of properties in the composite electrolyte increases the power of a thermo-electrochemical cell by about 30%.

Manuscript submitted April 14, 2016; revised manuscript received May 26, 2016. Published June 7, 2016.

In the 1980s, thermo-electrochemical cells (thermocells) along with other photo-converters were heralded as potential technologies for solar energy conversion.[1–3] Recent interest in thermocells has been sparked by concern over the environmental impact of fossil fuels, the finite supply of fossil fuels and the need to use these remaining resources efficiently.[4] More importantly, processes powered by combustion of fossil fuels lose 63.9% of energy in the form of heat,[5] making technologies that scavenge heat an absolute necessity. Additionally, miniaturization of devices and their low power requirements has developed a new niche market of utilizing ambient heat as an indigenous power source. Thermocells convert thermal energy to electrical energy using a chemical reaction of ions at the electrodes. In contrast, solid-state thermoelectrics convert a temperature difference to electric voltage using electrons and holes as charge carriers. Compared to thermocells, thermoelectrics typically have higher cost along with material and physical limitations[6] including lower thermal energy to voltage conversion.[7] The recent advance of using multiwall carbon nanotubes (MWCNTs)[8,9] and single wall carbon nanotube (SWCNTs) combined with reduced graphene oxide (RGO),[10] has greatly reduced the cost of thermocells. Also, with the fabrication of carbon nanotube aerogel sheet electrodes power as high as 6.6 W/m^2 has been reported.[11] In addition, an earlier limitation of operating temperatures above 100°C has also been addressed by use of ionic liquids as the redox electrolyte.[12] The recent developments addressing the costs and material limitations makes thermocells economically more feasible and operational to temperatures up to 200°C.

In a thermocell (Fig. 1), a thermo electrochemical force (EMF) is generated by the free energy difference of products and reactants when a temperature difference is applied at the electrodes. The products after being oxidized/reduced migrate to opposite electrodes inside the electrolyte, meanwhile the electrons generated at the anode due to the oxidation of ions flow through the external circuit from anode to cathode. For aqueous electrolyte water molecules carry heat from hot to cold side.

The influence of temperature on the EMF generated is known as the Seebeck effect, represented by Seebeck coefficient S_e. S_e is related to reaction entropy of the redox reaction by the following relation:

$$S_e = \frac{\partial E(T)}{\partial T} = \frac{\Delta S}{nF} \quad [1]$$

Where E(T) is equilibrium electrode potential, ΔS is the standard redox reaction entropy, n is the number of electrons involved in the reaction and F is the Faraday constant.[13,14] A high Seebeck coefficient, which gives a high equilibrium potential for a given temperature, is one of the requirements for a high energy conversion efficiency.[2] The other requirement are low ohmic, mass and charge transfer over potentials.[2,15] These over potentials are shown as resistances in Fig. 2. Also, the ratio of the flux of charge carriers to the flux of heat flowing between electrodes should be as high as possible.[3] By decreasing the thermal conductivity of the electrolyte, heat flux is decreased. This increases the ratio of charge carriers to heat flux and helps in improving the efficiency of thermocell.

In our previous work, we showed that addition of MWCNTs to ionic liquid electrolyte can reduce mass transfer resistance and increase power output.[16] However, the viscosity of ionic liquids is at least an order of magnitude greater than that of water,[17] which decreases the rate of ion diffusion and hence the ohmic conductivity of the electrolyte.[16] The highest ionic conductivity of ionic liquid is much lower than aqueous electrolyte,[18] thus conventional 0.4 M ferri/ferrocyanide ($[Fe(CN)_6]^{3-}$/$[Fe(CN)_6]^{4-}$) remains a first choice electrolyte for thermocells. In this paper, we mix 0.4 M $[Fe(CN)_6]^{3-}$/$[Fe(CN)_6]^{4-}$ with MWCNTs and poly(3,4-ethylenedioxythiophene):poly(styrenesulfonate) (PEDOT:PSS) to form a novel composite electrolyte. Nanoparticle addition to liquid electrolyte has been shown to reduce interfacial charge transfer resistance in previous studies.[19–22] Carbon nanotubes (CNTs) have been previously shown to disperse in stabilizers such as polymers[23–25] and surfactants.[26,27] Recently PEDOT:PSS has also been shown to stabilize and disperse CNTs in water. The conjugated polymer

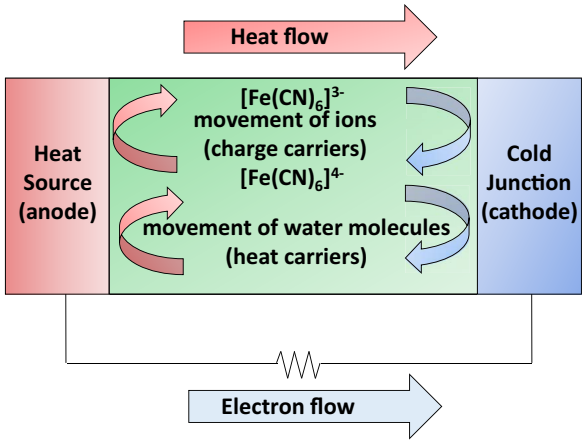

Figure 1. Schematic of thermocell showing the the flow of heat and electrons, movement of ions and water molecules for ferri/ferricyanide electrolyte.

*Electrochemical Society Student Member.
**Electrochemical Society Member.
[z]E-mail: cola@gatech.edu

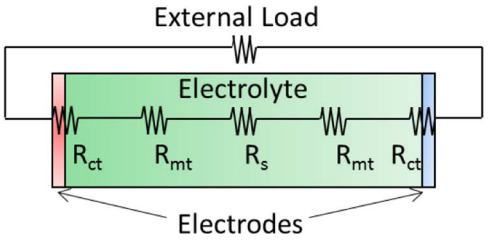

Figure 2. Schematic of over potential represented as resistances. R_s is ohmic resistance, R_{ct} is interfacial charge transfer resistance and R_{mt} is mass transfer resistance.

wraps around CNTs preventing aggregation and settling.[28,29] Combining the physicochemical properties of conjugated polymer and long range ballistic electrical conduction of CNTs have already been used in thermoelectrics,[30] dye-sensitized solar cells,[31,32] organic thin film transistors,[33] organic photovoltaics[33] and organic light emitting diodes[34] to improve their performance and reduce cost.[33] In the aforementioned devices the composite is used either as a film or electrode, but in this work for the first time the composite is dispersed in an aqueous system having a redox couple $[Fe(CN)_6]^{3-}/[Fe(CN)_6]^{4-}$.

We report an increase in ohmic conductivity (decrease in ohmic over potential) of aqueous redox electrolyte by the introduction of PEDOT:PSS and MWCNTs. We also report up to a 5 times decrease in interfacial charge transfer resistance in this composite electrolyte. We show that for aqueous based thermocells, increases in ohmic conductivity and reduction in interfacial charge transfer resistance with the new composite electrolyte produce a significant increase in power output.

Experimental

Materials and preparation.—MWCNTs (US4315) manufactured from chemical vapor deposition were purchased from US Research Nanomaterials, Inc. According to product specifications the purity is greater than 95% (from thermogravimetric analysis and transmission electron microscopy), the outside diameters are 50–80 nm, the lengths are 10–20 um and the density is 2.1 g/cm^3. PEDOT:PSS (PH1000) highly conductive homogenized dispersion was purchased from Heraeus Clevios. According to product specifications the solid content is 1–1.3%, viscosity is 15–50 mPas, the PEDOT:PSS ratio by weight is 1:2.5 at 20°C and the density is 1 g/cm^3. Potassium hexacyanoferrate (II) trihydrate and Potassium ferricyanide (III) were purchased from Sigma Aldrich having a molecular weight of 422.39 g/mol and 329.26 g/mol, respectively.

Mixtures of PEDOT:PSS and water were made by stirring for 30 min. MWCNTs were dispersed at different ratios in PEDOT:PSS dispersions by 30 min of stirring, 30 min of sonication and then 15 min of stirring. Composites of MWCNT and PEDOT:PSS prepared in the previous step were dispersed in $[Fe(CN)_6]^{3-}/[Fe(CN)_6]^{4-}$ by 30 min of stirring, 30 min of sonication and then 15 min of stirring. The sonication was done using an ultrasonic bath having a frequency of 40 kHz and stirring was done using magnetic stirrer at a speed of 1200 rpm. All steps were performed at ambient temperature.

Electrochemical impedance spectroscopy.—Electrochemical impedance spectroscopy (EIS) and modelling was performed using the procedure used in our previous work.[16] Briefly, two platinum electrodes were used in the electrochemical setup. EIS was performed using CH instruments model 660E potentiostat in the spectral range 1 MHz–0.02 Hz, with an AC amplitude of 20 mV and DC signal of 0 mV. The collected data was fitted using the software provided by CH instruments. Randles model was used to compute ohmic resistance, R_s, interfacial charge transfer resistance, R_{ct}, Warburg or diffusion impedance, W, and double-layer capacitance, C_{dl}. The Randles equivalent circuit helps in separating the behavior in the bulk solution from that at the interface. R_s was used to calculate ohmic conductivity, σ, of the electrolyte by calibrating it with 0.1 M and 1 M standard solution of potassium chloride as shown in our previous work.[16,35]

Cyclic voltammetry.—Cyclic Voltammetry (CV) was performed using three-electrode cell configuration. The working and counter electrode were of Platinum while the reference electrode Ag/AgCl. CV sweeps were performed using CH instrument model 660E potentiostat for the range −0.3 to 0.7 V using a scan rate 0.1 V/s. For each sample CV sweep was recorded for temperature range 293 to 353 K, having 5 K increment. CV was used to calculate ΔS, S_e and to observe the shift in half-wave potential ($E_{1/2}$) with temperature using the method described previously.[36,37]

Thermocell measurements.—A T-shaped cell was used to perform thermocell testing for temperature differences (ΔT) of 20, 40, 60, 80 and 100 K between the heating and cooling blocks. Graphite electrodes having a cross-sectional area of 0.08 cm^2 were used as the two electrodes. The heating block is heated by two Omega 7750 W/m^2 silicones rubber heaters. The cooling block is maintained at ambient temperature by the environment. The performance of 0.4 M $[Fe(CN)_6]^{3-}/[Fe(CN)_6]^{4-}$ electrolyte was compared with the same electrolyte with different concentrations of PEDOT:PSS and PEDOT:PSS/MWCNT composites. The thermocell testing was done with a potentiostat by recording open circuit voltage and short circuit current. The measurements were repeated after 12 hour intervals to check for stability.

Results and Discussion

Electrochemical impedance spectroscopy.—In order to introduce MWCNTs and PEDOT:PSS to the aqueous redox electrolyte, a systematic procedure was followed. First, the PEDOT:PSS dispersion was added to water and an increase in ohmic conductivity was measured (Table S1). The increase is ohmic conductivity is seen because PEDOT:PSS is a conductive polymer having positive and negative ions. Increasing the amount of PEDOT:PSS increases the number of ions in distilled water and hence reduces the ohmic resistance R_s.

The next step was to add PEDOT:PSS to aqueous 0.4 M $Fe(CN)_6]^{3-}/[Fe(CN)_6]^{4-}$ (Figs. 3 and S1). This increases the ohmic conductivity, which is attributed to the addition of the ions present in

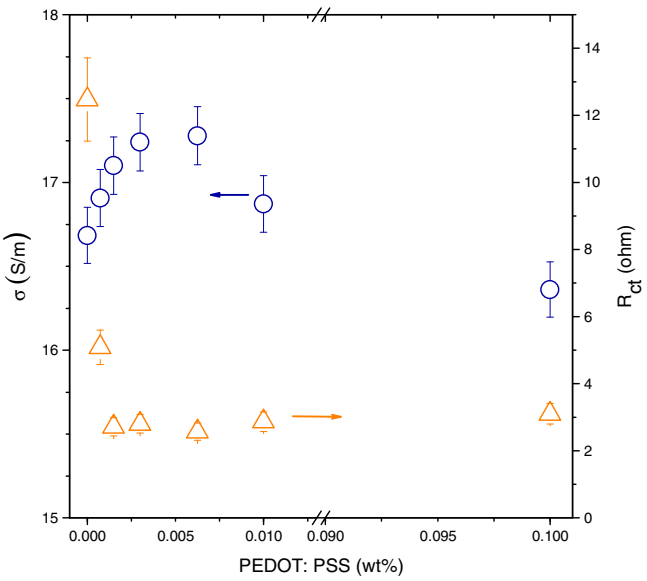

Figure 3. Effect of increasing PEDOT:PSS (wt%) on conductivity and interfacial charge transfer resistance of 0.4 M $[Fe(CN)_6]^{3-}/[Fe(CN)_6]^{4}$. σ is the ohmic conductivity of the solution (blue circle), R_{ct} is the interfacial charge transfer resistance (orange triangle).

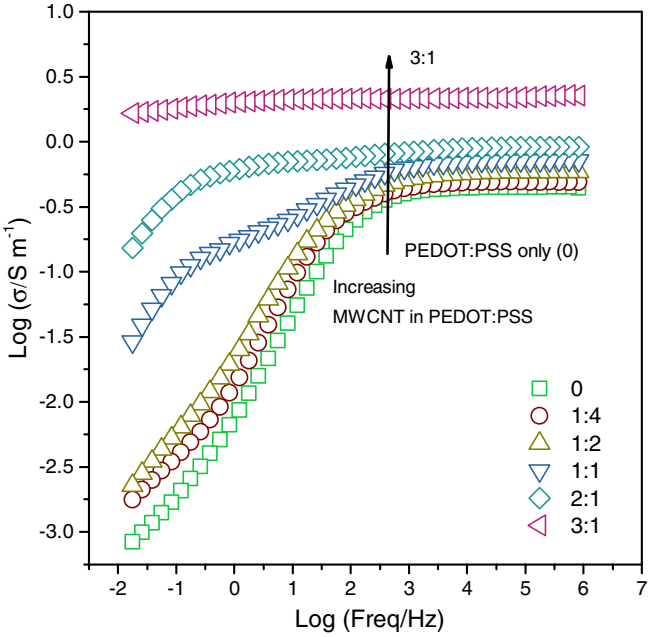

Figure 4. Frequency dependence of impedance at increasing concentration ratio of MWCNT, 0 (green) only PEDOT:PSS, MWCNT:(PEDOT:PSS) varying from 1:4 (wine) to 3:1 (pink).

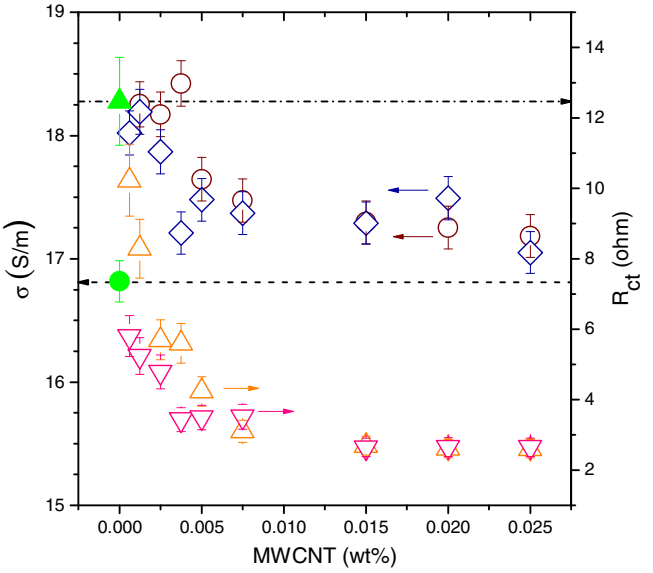

Figure 5. Effect of MWCNT, PEDOT:PSS composite on 0.4 M $[Fe(CN)_6]^{3-}$/$[Fe(CN)_6]^{4-}$. MWCNT:(PEDOT:PSS) 1:4 in 0.4 M $[Fe(CN)_6]^{3-}$/$[Fe(CN)_6]^{4-}$ σ (blue diamond) and R_{ct} (pink down triangles), MWCNT: (PEDOT:PSS) 3:1 in 0.4 M $[Fe(CN)_6]^{3-}$/$[Fe(CN)_6]^{4-}$ σ (brown circles) and R_{ct} (yellow triangles). Upper dash dot line is the initial value of R_{ct} correspond to green solid triangle, lower dash line is the initial value of σ correspond to green solid circle. Both green solid triangle and green solid circle correspond to 0 wt% MWCNT in the composite.

PEDOT:PSS. However, higher concentration of 0.1 wt% PEDOT:PSS suppresses the ohmic conductivity, probably because the effect of increase in number ions is offset by increase in viscosity of the mixture.[16,20,35] In addition, interfacial charge transfer resistance is decreased significantly (Fig. 3). This shows that increase in conductive polymer not only increases the bulk transport of redox couple but also increases the rate of charge transfer at the electrode. This implies that increasing wt% of conductive polymer improves contact between the electrode and electrolyte.

The effect of MWCNTs on the PEDOT:PSS dispersion is shown in Fig. 4. A gradual increase in conductivity is observed over the entire frequency range for each increment of MWCNT concentration. For small concentration of MWCNT the spectrum shifted slightly maintaining its shape, however at higher concentrations of MWCNTs the change in spectrum was more significant, especially at lower frequency. It has been shown that polymer helps disrupt the CNT hydrophobic interaction with water and also disrupts the CNT-CNT interaction, which prevents aggregation.[38] This behavior helps in dispersing CNTs in polymer, forming a composite, which later can be dispersed in electrolyte. Conjugated polymers have been known to display good binding with CNTs; in the absence of chemical functionalization the polymer CNT interaction is solely by van der Waals forces.[39,40,41] The MWCNTs were added to a high 3:1 ratio MWCNT:(PEDOT:PSS). The increase in conductivity shows the creation of percolated networks and interfacial polarization[16] that facilitate charge transfer. At a higher MWCNT concentration the spectra matches that of a resistor (i.e., frequency independent).

Finally, the electrolyte composite of MWCNTs and PEDOT:PSS was added to 0.2 M $Fe(CN)_6]^{3-}$/$[Fe(CN)_6]^{4-}$ (Tables S2 and S3) and 0.4 M $Fe(CN)_6]^{3-}$/$[Fe(CN)_6]^{4-}$ (Figs. 5 and S2). Ohmic conductivity of 0.4 M $Fe(CN)_6]^{3-}$/$[Fe(CN)_6]^{4-}$ (Fig. 5) is about 1.7 times greater than that of 0.2 M $Fe(CN)_6]^{3-}$/$[Fe(CN)_6]^{4-}$(Tables S2 and S3). For both the lean (4 times less than PEDOT:PSS) and rich (3 times more than PEDOT:PSS) mixtures of MWCNT similar trends of R_{ct} and σ were observed. A slight increase in ohmic conductivity was observed, while the decrease in interfacial charge transfer resistance was much more significant for both mixtures. Lean mixture of MWCNT had a maximum increase of 8% in ohmic conductivity for 0.00125 wt% of MWCNT (PEDOT:PSS 0.005 wt%). Also, for the same ratio, about a 5 times decrease in interfacial charge transfer resistance was observed for 0.015 wt% of MWCNT. As for the rich MWCNT mixture about 10% increase in ohmic conductivity was observed for 0.00375 wt% of MWCNT and about a 5 times decrease in interfacial charge transfer resistance for 0.025 wt% of MWCNT. The increase in ohmic conductivity can be attributed to the addition of ions present in PEDOT:PSS and the interfacial polarization due to dispersed MWCNT.[16]

MWCNTs dispersed in PEDOT:PSS added to an electrolyte increase the interfacial area where dipoles can orient and hence increasing the ohmic conductivity.[35] Once the temperature difference is applied at the electrodes, a potential difference is generated at the electrodes causing ions to migrate and charges on MWCNTs to reorient. Reorientation of charges on the MWCNT helps in the migration of ions to charged surfaces (interfacial polarization) resulting in increase in ohmic conductivity. The decrease in interfacial charge transfer resistance implies that nanoparticle addition improves contact between the electrode and the electrolyte.

Cyclic voltammetry.—Temperature dependent cyclic voltammetry was performed on 0.4 M $[Fe(CN)_6]^{3-}$/$[Fe(CN)_6]^{4-}$ (Figs. 3 and S3a) and compositions determined in the previous section corresponding to 0.00625 wt% of PEDOT:PSS (Figs. 3 and S3b) lean and rich mixture corresponding to 0.015 wt% of MWCNT (Figs. 5, S3c and S3d). The slope of $E_{1/2}$ versus temperature (Fig. 6), which corresponds to S_e is −1.5 mV/K for all electrolyte types and the corresponding ΔS is −144.7 J K^{-1} mol^{-1}, which is consistent with literature.[42,43] Notably, the downward shift $E_{1/2}$ suggest increase preference of the redox couple toward formation of $[Fe(CN)_6]^{3-}$ (the equilibrium move to right in the following equation) in sample having carbon nanotube and polymer composite.[36,44]

$$\left[Fe(CN)_6\right]^{4-} \leftrightarrows \left[Fe(CN)_6\right]^{3-} + e^- \qquad [2]$$

This effect is same as having a higher average temperature in the cell because as the temperature is increased $E_{1/2}$ decreases.

T-cell thermocell testing.—The performance of thermocells having aqueous composite electrolyte was tested in T-cell thermocell configuration (Fig. 7). The electrolyte composition was based on

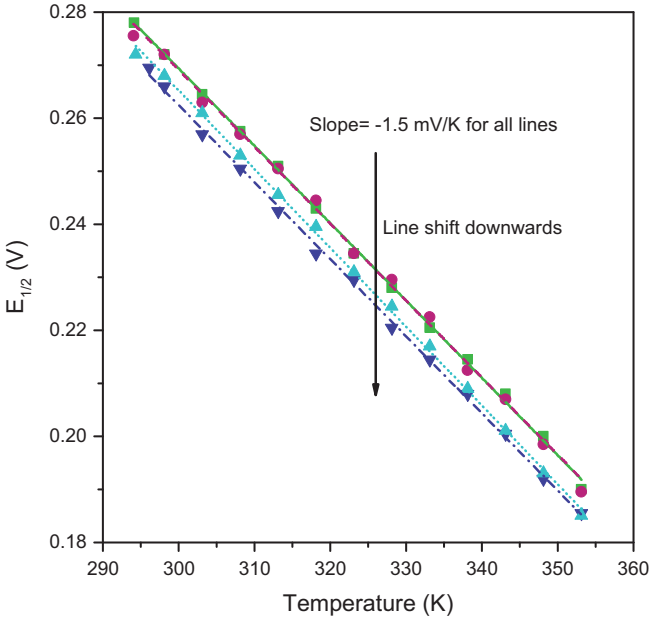

Figure 6. Half-wave potential of 0.4 M $[Fe(CN)_6]^{3-}/[Fe(CN)_6]^{4-}$ (green square), 0.4 M $[Fe(CN)_6]^{3-}/[Fe(CN)_6]^{4-}$ + 0.00625 wt% PEDOT:PSS (pink circle), 0.4 M $[Fe(CN)_6]^{3-}/[Fe(CN)_6]^{4-}$ + 0.06 wt% PEDOT:PSS + 0.015 wt% MWCNT (blue triangle up), 0.4 M $[Fe(CN)_6]^{3-}/[Fe(CN)_6]^{4-}$ + 0.005 wt% PEDOT:PSS + 0.015 wt% MWCNT (purple triangle down) as a function of temperature of isothermal cell.

the enhancement in ohmic conductivity and reduction in interfacial charge transfer resistance after the introduction of polymer and MWCNT composite. The temperature difference used in the calculation is the difference in temperatures of the heating and cooling blocks and not the temperature difference at the electrodes. To prevent leakage from cell, the thermocouple could not be placed at the electrodes. The temperature difference of the blocks recorded is higher than what is present at the electrodes due to thermal resistance losses. The higher temperature difference measured at the heating and cooling blocks results in a $V_{oc}/\Delta T$ less than 1.5 mV/K (Fig. 8a), which is the seebeck coefficient recorded in the previous section. A power performance comparison for electrolyte having a

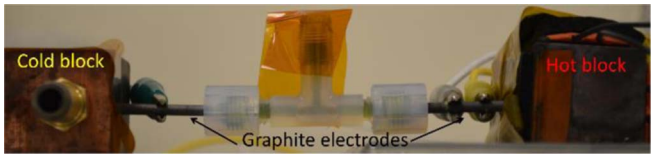

Figure 7. Photograph of t-shape thermocell experimental setup to generate power.

lean (more PEDOT:PSS), rich (less PEDOT:PSS) and no MWCNT mixture (only PEDOT:PSS) is compared with that of electrolyte with only 0.4 M $Fe(CN)_6]^{3-}/[Fe(CN)_6]^{4-}$ (Fig. 8). Each of the particle additions increased the $V_{oc}/\Delta T$ compared to pristine electrolyte. (PEDOT:PSS):MWCNT 1:3 produced the greatest increase in $V_{oc}/\Delta T$. This can be attributed to decrease in interfacial charge transfer resistance of the composite, which helps in increasing the V_{oc}.[21] The cell conductance J_{sc}/V_{oc} has a positive slope because the J_{sc} increase with each increment of ΔT is not matched by a corresponding proportionate increase in V_{oc}. Comparing the lean and rich mixture, the wt% of MWCNT was fixed at 0.015 wt% with PEDOT:PSS amount 0.06 wt% and 0.005 wt% respectively. The lower wt% of PEDOT:PSS improves the performance, while increasing the wt% of PEDOT:PSS increases viscosity which counteracts the positive effect of increase in PEDOT:PSS ions as the interfacial charge transfer resistance and ohmic conductivity is same for both mixtures at 0.015 wt% of MWCNT (Fig. 5). However, for both composites having MWCNTs, the power measured is more than without the MWCNTs. The overall increase in power output is about 1.30 times greater than without the composite for a ΔT of 40 K for MWCNT rich composite. The highest power achieved with composite was 0.5 W/m^2 for a ΔT of 100 K. The overall enhancement in performance is a combination of reduction in interfacial charge transfer resistance, increase in ohmic conductivity and increase in interfacial polarization.

To test the stability of the enhancement, V_{oc} and J_{sc} for t-shape thermocell having rich mixture MWCNT were measured over a 30 day period (Fig. 9). The stable performance suggest that polymer and carbon nanotube composite electrolyte can be used for long term operation.

Conclusions

We have shown improvements in the electrochemical properties of the standard 0.4 M $Fe(CN)_6]^{3-}/[Fe(CN)_6]^{4-}$ aqueous electrolyte by introducing polymer and carbon nanotube composite, which increases

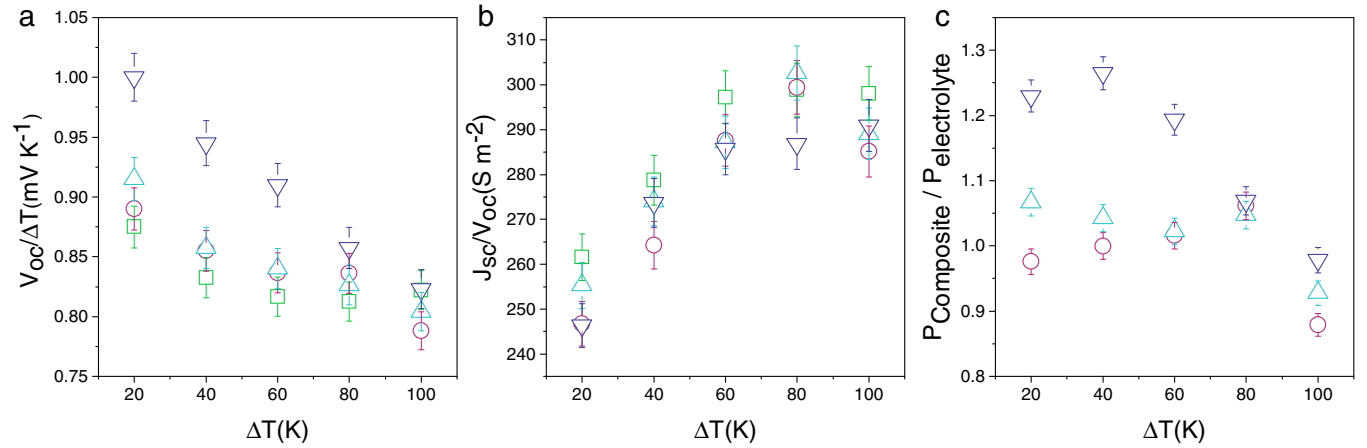

Figure 8. T-shaped thermocell performance using 0.4 M $[Fe(CN)_6]^{3-}/[Fe(CN)_6]^{4-}$ (green squares), 0.4 M $[Fe(CN)_6]^{3-}/[Fe(CN)_6]^{4-}$ + 0.00625 wt% PEDOT:PSS (pink circles), 0.4 M $[Fe(CN)_6]^{3-}/[Fe(CN)_6]^{4-}$ + 0.06 wt% PEDOT:PSS + 0.015 wt% MWCNT (blue triangles up), 0.4 M $[Fe(CN)_6]^{3-}/[Fe(CN)_6]^{4-}$ + 0.005 wt% PEDOT:PSS + 0.015 wt% MWCNT (purple triangles down) as a function of different temperature difference (ΔT). ΔT is the temperature difference between hot and cold block. (a) $V_{oc}/\Delta T$ is the ratio of the open circuit voltage and temperature difference. (b) J_{sc}/V_{oc} is the ratio of short current density and open circuit voltage. (c) $P_{composite}/P_{electrolyte}$ is the ratio of the maximum power measured with and without the composite.

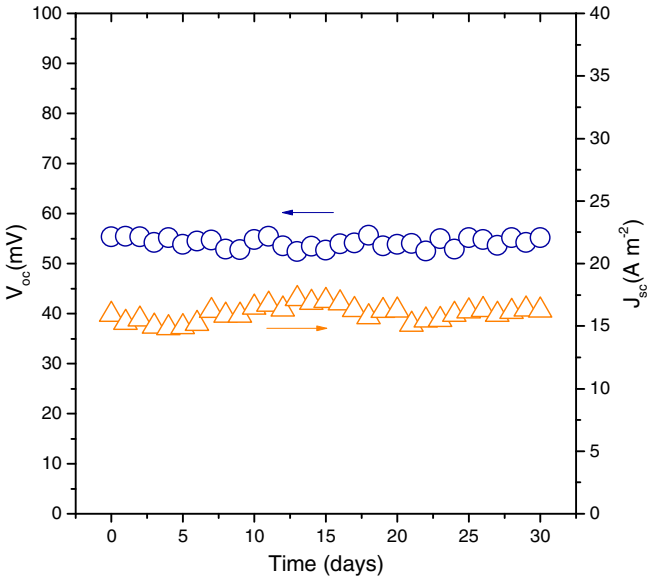

Figure 9. Performance of t-shape thermocell with polymer and carbon nanotube composite electrolyte versus time for ΔT approximately 60 K. Electrolyte composition 0.4 M $[Fe(CN)_6]^{3-}/[Fe(CN)_6]^{4-}$ + 0.005 wt% PEDOT:PSS + 0.015 wt% MWCNT. V_{oc} is the open circuit voltage (blue circle), J_{sc} is the short circuit current per unit cross-sectional area (orange triangle).

the ohmic conductivity and reduces the interfacial charge transfer resistance. The improvement in performance is observed by a systematic study of the effect of introducing first polymer only in the electrolyte and then introducing polymer: CNT lean (4:1) and rich (1:3) composites. In the absence of chemical functionalization the interaction between CNTs and polymer is through van der Waals forces, this interaction prevents CNT-CNT agglomeration and helps disperse CNTs in the polymer. Lean and rich composite dispersed in electrolyte were tested in t-shape thermocell, with rich CNT composite having the maximum power enhancement. The enhancement is attributed addition in number of ions present in PEDOT:PSS, interfacial polarization and improve contact at the electrode/electrolyte interface.

Acknowledgments

Financial support from National Science Foundation Award No. 1055479 is greatly acknowledged. A.H. Kazim is grateful for support from a Fulbright Fellowship. Sincere thanks to colleagues in the NEST Lab for useful suggestions and comments on the manuscript.

References

1. H. L. Chum and R. A. Osteryoung. *Solar Energy Research Inst., Golden, CO (USA)*; State Univ. of New York, Buffalo (USA), 1981.
2. T. Quickenden and C. Vernon, *Solar Energy*, **36**(1), 63 (1986).
3. T. Quickenden and Y. Mua, *Journal of The Electrochemical Society*, **142**(11), 3985 (1995).
4. T. M. Tritt, H. Böttner, and L. Chen, *MRS bulletin*, **33**(04), 366 (2008).
5. U.S. Department of energy, 2011.
6. C. B. Vining, *Nature Materials*, **8**(2), 83 (2009).
7. A. Gunawan, C. H. Lin, D. A. Buttry, V. Mujica, R. A. Taylor, R. S. Prasher, and P. E. Phelan, *Nanoscale and Microscale Thermophysical Engineering*, **17**(4), 304 (2013).
8. R. Hu, B. A. Cola, N. Haram, J. N. Barisci, S. Lee, S. Stoughton, G. Wallace, C. Too, M. Thomas, and A. Gestos, *Nano letters*, **10**(3), 838 (2010).
9. T. J. Kang, S. Fang, M. E. Kozlov, C. S. Haines, N. Li, Y. H. Kim, Y. Chen, and R. H. Baughman, *Advanced Functional Materials*, **22**(3), 477 (2012).
10. M. S. Romano, N. Li, D. Antiohos, J. M. Razal, A. Nattestad, S. Beirne, S. Fang, Y. Chen, R. Jalili, and G. G. Wallace, *Advanced Materials*, **25**(45), 6602 (2013).
11. H. Im, T. Kim, H. Song, J. Choi, J. S. Park, R. Ovalle-Robles, H. D. Yang, K. D. Kihm, R. H. Baughman, and H. H. Lee, *Nature communications*, **7** (2016).
12. D. R. MacFarlane, N. Tachikawa, M. Forsyth, J. M. Pringle, P. C. Howlett, G. D. Elliott, J. H. Davis, M. Watanabe, P. Simon, and C. A. Angell, *Energy Environ. Sci.*, **7**(1), 232 (2014).
13. Y. Mua and T. Quickenden, *Journal of The Electrochemical Society*, **143**(8), 2558 (1996).
14. T. J. Abraham, D. R. MacFarlane, R. H. Baughman, N. Li, Y. Chen, and J. M. Pringle, *in "MRS Proceedings"*, Vol. 1575, p. mrss13-1575-vv1504-1508. Cambridge Univ Press, 2013.
15. A. J. Bard and L. R. Faulkner, *Electrochemical methods: fundamentals and applications*, Wiley New York (1980).
16. P. F. Salazar, S. T. Stephens, A. H. Kazim, J. M. Pringle, and B. A. Cola, *Journal of Materials Chemistry A*, **2**(48), 20676 (2014).
17. D. Rooney, J. Jacquemin, and R. Gardas, *Top Curr Chem*, **290** 185 (2010).
18. M. Galiński, A. Lewandowski, and I. Stępniak, *Electrochimica Acta*, **51**(26), 5567 (2006).
19. T. Katakabe, R. Kawano, and M. Watanabe, *Electrochemical and solid-state letters*, **10**(6), F23 (2007).
20. H. F. Lee, J. L. Wu, P. Y. Hsu, Y. L. Tung, F. Y. Ouyang, and J. J. Kai, *Thin Solid Films*, **529** 2 (2013).
21. C. P. Lee, K. M. Lee, P. Y. Chen, and K. C. Ho, *Solar Energy Materials and Solar Cells*, **93**(8), 1411 (2009).
22. T. Kato, T. Kado, S. Tanaka, A. Okazaki, and S. Hayase, *Journal of the Electrochemical Society*, **153**(3), A626 (2006).
23. Y. Dror, W. Pyckhout-Hintzen, and Y. Cohen, *Macromolecules*, **38**(18), 7828 (2005).
24. J. C. Grunlan, L. Liu, and O. Regev, *Journal of colloid and interface science*, **317**(1), 346 (2008).
25. J. Ouyang, Q. Xu, C.-W. Chu, Y. Yang, G. Li, and J. Shinar, *Polymer*, **45**(25), 8443 (2004).
26. O. Matarredona, H. Rhoads, Z. Li, J. H. Harwell, L. Balzano, and D. E. Resasco, *The Journal of Physical Chemistry B*, **107**(48), 13357 (2003).
27. V. C. Moore, M. S. Strano, E. H. Haroz, R. H. Hauge, R. E. Smalley, J. Schmidt, and Y. Talmon, *Nano Letters*, **3**(10), 1379 (2003).
28. J. N. Coleman, U. Khan, W. J. Blau, and Y. K. Gun'ko, *Carbon*, **44**(9), 1624 (2006).
29. B. McCarthy, J. Coleman, R. Czerw, A. Dalton, M. In Het Panhuis, A. Maiti, A. Drury, P. Bernier, J. Nagy, and B. Lahr, *The Journal of Physical Chemistry B*, **106**(9), 2210 (2002).
30. C. Yu, K. Choi, L. Yin, and J. C. Grunlan, *ACS nano*, **5**(10), 7885 (2011).
31. W. Hong, Y. Xu, G. Lu, C. Li, and G. Shi, *Electrochemistry Communications*, **10**(10), 1555 (2008).
32. M. B. Achari, V. Elumalai, N. Vlachopoulos, M. Safdari, J. Gao, J. M. Gardner, and L. Kloo, *Physical Chemistry Chemical Physics*, **15**(40), 17419 (2013).
33. D. J. Yun, K. Hong, S. Kim, W. M. Yun, J. Y. Jang, W. S. Kwon, C. E. Park, and S. W. Rhee, *ACS Appl Mater Interfaces*, **3**(1), 43 (2011).
34. J. Park, A. Lee, Y. Yim, and E. Han, *Synthetic Metals*, **161**(5–6), 523 (2011).
35. P. F. Salazar, K. J. Chan, S. T. Stephens, and B. A. Cola, *Journal of The Electrochemical Society*, **161**(9), H481 (2014).
36. N. G. Tsierkezos, *Journal of Solution Chemistry*, **36**(3), 289 (2007).
37. P. F. Salazar, *in* "PhD thesis, Georgia Institute of Technology". *PhD thesis*, Georgia Institute of Technology, 2014.
38. M. J. O'Connell, P. Boul, L. M. Ericson, C. Huffman, Y. Wang, E. Haroz, C. Kuper, J. Tour, K. D. Ausman, and R. E. Smalley, *Chemical physics letters*, **342**(3), 265 (2001).
39. M. Yang, V. Koutsos, and M. Zaiser, *The Journal of Physical Chemistry B*, **109**(20), 10009 (2005).
40. M. Wong, M. Paramsothy, X. Xu, Y. Ren, S. Li, and K. Liao, *Polymer*, **44**(25), 7757 (2003).
41. K. Liao and S. Li, *Applied Physics Letters*, **79**(25), 4225 (2001).
42. J. T. Hupp and M. J. Weaver, *Inorganic Chemistry*, **23**(22), 3639 (1984).
43. P. F. Salazar, S. Kumar, and B. A. Cola, *Journal of The Electrochemical Society*, **159**(5), B483 (2012).
44. N. G. Tsierkezos and U. Ritter, *The Journal of Chemical Thermodynamics*, **54** 35 (2012).

Figure S2: Electrochemical impedance spectra of increasing MWCNT (wt%) on 0.4 M $[Fe(CN)_6]^{3-}$ /$[Fe(CN)_6]^{4-}$ using MWCNT:(PEDOT:PSS) 1:4 composite(a) , MWCNT: (PEDOT:PSS) 3:1 (b). Insets show an enlarge scale

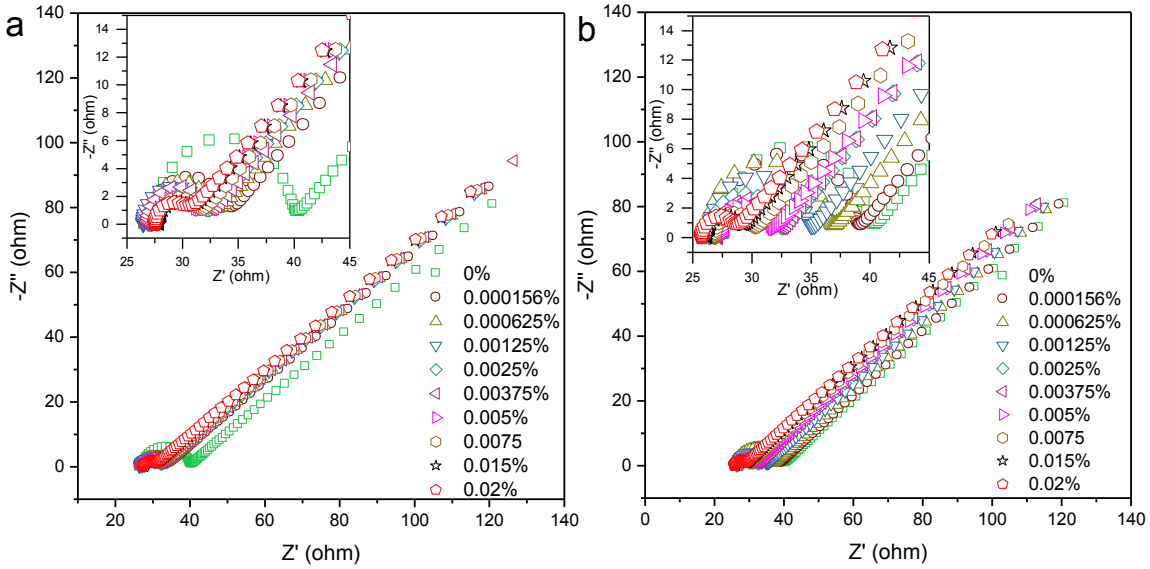

Cyclic Voltammetry

Figure S2: Cyclic Voltammetry of 0.4 M $[Fe(CN)_6]^{3-}/[Fe(CN)_6]^{4-}$ (a), 0.4 M $[Fe(CN)_6]^{3-}/[Fe(CN)_6]^{4-}$ + 0.00625 wt% PEDOT:PSS (b), 0.4 M $[Fe(CN)_6]^{3-}/[Fe(CN)_6]^{4-}$ + 0.06 wt% PEDOT:PSS + 0.015 wt% MWCNT (c), 0.4 M $[Fe(CN)_6]^{3-}/[Fe(CN)_6]^{4-}$ + 0.005 wt% PEDOT:PSS + 0.015 wt% MWCNT (d) as function isothermal cell temperature 20 ^{o}C (black), 30 ^{o}C (red), 40 ^{o}C (blue), 50 ^{o}C (magenta), 60 ^{o}C (olive), 70 ^{o}C (navy), 80 ^{o}C (violet). As temperature is increased peaks shift to the left and current increases. The half-wave potential also shifts to left (decreases) for (b), (c), (d) compare to (a) as shown in Figure 6 of main text.

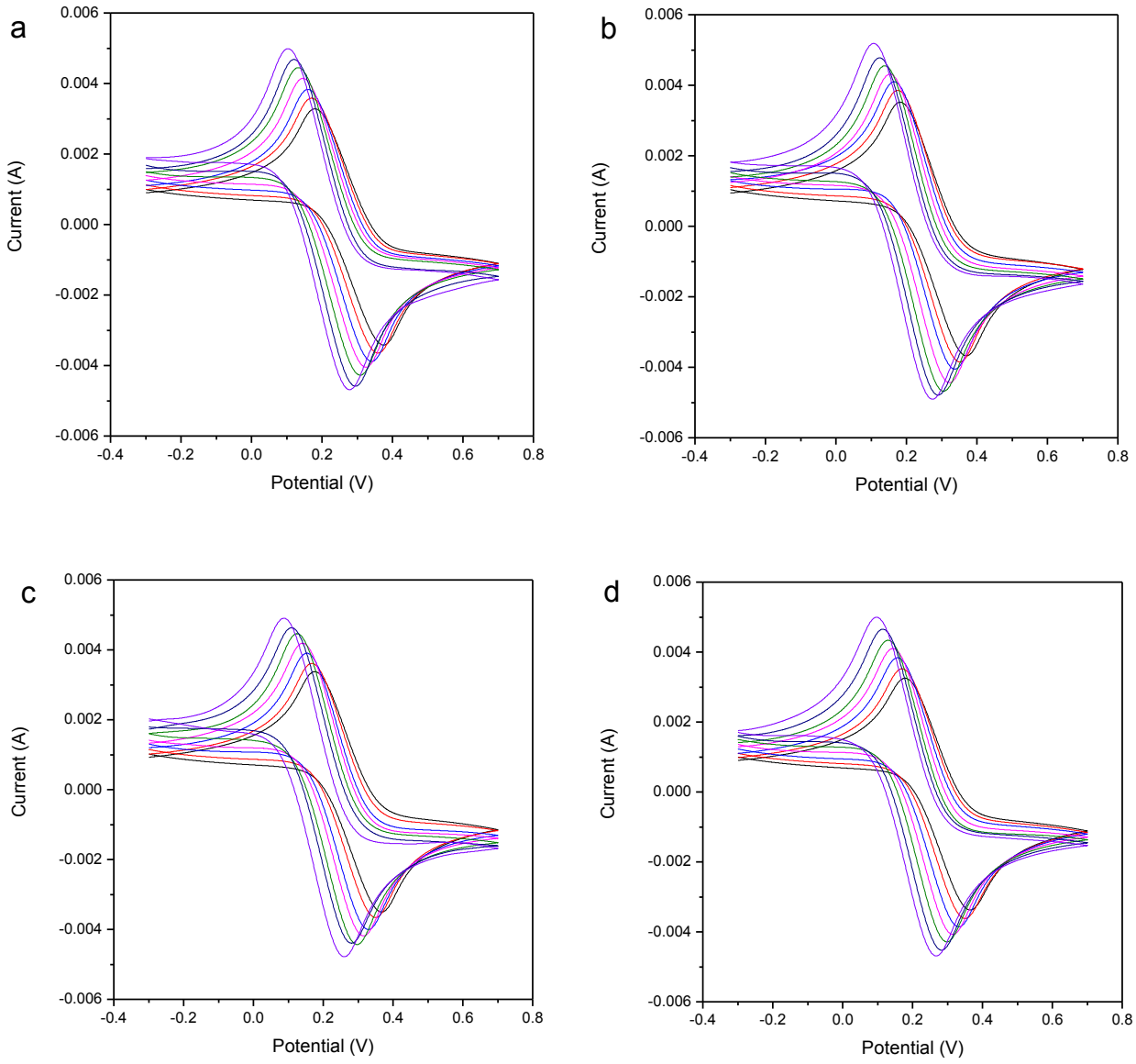

Calculating Seebeck coefficient

Cyclic Voltammetry was performed using three-electrode cell configuration as described in main text. All potentials were recorded with reference to Ag/AgCl reference electrode (Figure S3). Anodic peak (E_{pa}) and cathodic peak (E_{pc}) potentials were obtained using the software provided by CH instrument. Half-wave potential ($E_{1/2}$) is determined as follows:

$$E_{1/2} = \frac{E_{pa} + E_{pc}}{2} \quad [1]$$

Half-wave potential was measured versus temperature and plotted as shown in Figure 6. The slope of the graph gives the Seebeck coefficient and can be shows as follows:

$$S_e = \frac{(E_{1/2})_{T_1} - (E_{1/2})_{T_2}}{T_1 - T_2} \quad [2]$$

Where $(E_{1/2})_{T_1}$ and $(E_{1/2})_{T_2}$ are half-wave potential measured at temperatures T_1 and T_2 respectively.